

Full-wave Electromagnetic Analysis of Lightning Strikes to Wind Farm Connected to Medium-Voltage Distribution Lines

Wagner Costa da Silva, Walter Luiz Manzi de Azevedo, Anderson Ricardo Justo de Araújo, José Pissolato Filho

Abstract—This paper studies the voltages developed on a wind turbine (WT) and a medium-voltage distribution line (MVDL) connected to a wind farm subjected to lightning strikes and located on FD (FD) soils. The ground potential rise (GPR), voltages at the blade tip and on phase conductors of the MVDL are calculated using the full-wave electromagnetic software XGSLab[®] employing the rigorous Partial Element Equivalent Circuit (PEEC) method. The wind farm comprises four wind turbines with interconnected grounding systems using cables buried in resistivity soils of 1,000 and 5,000 $\Omega\cdot\text{m}$. The voltages are computed for the first positive impulse (FPI) of 100-kA 10/350 μs and for the subsequent negative impulse (SNI) of 50-kA, 1/200 μs . Results have shown that voltage peaks increase notably as the soil resistivity increases. When the WTs are assumed, oscillations in the GPR waveforms for the SNI occur due to the multiple reflections between the blade and the turbine's base. However, the voltages for the FPI present smooth time-domain responses. Furthermore, the overvoltages developed at the MVDL are significantly dependent on the soil resistivity and lightning current waveform.

Keywords—Electromagnetic transients, grounding systems, lightning performance, soil modeling, wind turbines

I. INTRODUCTION

Due to the fast and continued growth of the electricity demand, wind turbines (WTs) have been installed worldwide to generate renewable and clean energy to supply this necessity. To achieve this objective, the turbine has increased height to provide power systems more energy. Additionally, a wind farm (WF) consisting of a large system of multiple WTs electrically interconnected is often employed to extract maximum power in a particular area. However, lightning protection on a tall WT, especially for those structures installed on high terrains or hilltops, has presented many challenges to engineers [1], [2]. Tall WTs (more than 150 m in height,

in general) are more vulnerable to lightning strokes during thunderstorms, and also, these structures can be excellent lightning initiators [2]. Besides that, many components such as sensible electronic equipment, generator, and transformer located in the nacelle can be exposed to dangerous voltages [3], [4], [5]. At the tower base, the ground potential rise (GPR) developed for the fast-front lightning currents at the grounding system of the WT must guarantee the protection of people and reduce the damages to the installations and equipment in the vicinity during the transient state [6], [7].

If the WF is large and is located far from the AC substation, the WTs can be directly connected to the power grid using a transformer to elevate the voltage from the generator up to the medium voltage of the distribution system [8]. For this purpose, the nacelle is equipped with transformers connected to the medium-voltage distribution line (MVDL) by insulated cables. Moreover, the transformer is inside the nacelle to reduce losses and increase efficiency [8]. These transformers also use the dry-type technology because of the limited space within the nacelle [1]. In this context, modeling the WF concerning the aerial elements (blades, nacelle, tower) with the interconnected grounding system (GS) must be appropriately carried out to precisely compute the transient voltages generated by lightning strikes. Recently, many works have studied WTs, and WFs [3], [6], [9]. In [3], the authors implemented a WT circuit in software ATP and calculated the transient voltages using a hybrid approach based on electromagnetic field theory for the grounding system and a lumped circuit representation of the WT. In [2], the authors presented the experimental and analytical results of a reduced-scale wind turbine using FDTD focusing on the overvoltages generated by lightning strikes. In [10], the authors investigate the induced overvoltages on the MVDL located on frequency-dependent (FD) soil for lightning striking at the tip of the blade. In [9], the authors analyzed the impact of FD soil with variable content on the transient voltages on different parts of a WT assuming vertical bars as the grounding system.

This paper investigates the transient voltages developed on a WT and an MVDL near a wind farm. The WF is located on soil whose electrical parameters are FD modeled by recommended expressions from CIGRE WG [11]. The ground potential rise (GPR), voltages at the tip of the blade (striking point) and on the medium-voltage distribution line are calculated employing the full-wave electromagnetic software XGSLab[®][12] using the Partial Element Equivalent Circuit (PEEC) method. The WF comprises four WTs whose

This work was supported by the Coordenação de Aperfeiçoamento de Pessoal de Nível Superior (CAPES) - Finance code 001 and by São Paulo Research Foundation (FAPESP) (grant: 2019/01396-1).

Wagner Costa da Silva is with the School of Electrical and Computer Engineering (FEEC), University of Campinas, Campinas, Brazil (e-mail: w223738@dac.unicamp.br).

Walter Luiz Manzi de Azevedo is with the School of Electrical and Computer Engineering (FEEC), University of Campinas, Campinas, Brazil (e-mail: w157573@unicamp.br).

Anderson Ricardo Justo de Araújo is with the School of Electrical and Computer Engineering (FEEC), University of Campinas, Campinas, Brazil (e-mail of the corresponding author: ajaraujo@unicamp.br).

José Pissolato Filho is with the School of Electrical and Computer Engineering (FEEC), University of Campinas, Campinas, Brazil (e-mail: pisso@unicamp.br).

Paper submitted to the International Conference on Power Systems Transients (IPST2023) in Thessaloniki, Greece, June 12-15, 2023.

grounding systems are interconnected by underground cables buried in soils with two resistivity values of 1,000 and 5,000 $\Omega\cdot\text{m}$. All the transient responses are calculated for two lightning currents: an FPI of 100 kA 10/350 μs and an SNI of 50-kA, 1/200 μs , both modeled by Heidler's function according to IEC 61400-24 [13]. Results have demonstrated that voltage peaks increase notably as the soil resistivity increases. When the wind turbine is considered, the voltages have oscillatory behavior for the SNI due to the multiple reflections of the surge waves between the tip and the base of the wind turbine. However, when the FPI 10/350 μs is considered, the voltages present smooth behavior. Furthermore, the overvoltages developed at the distribution line strongly depend on the soil resistivity and lightning current waveform. This work is based on a real WF connected to a medium-voltage distribution line located in the North-east region of Brazil. To the authors' knowledge, this is the first study of lightning performance combining wind farms connected to distribution lines. This paper provides a complete WF modeling using the full-wave electromagnetic software XGSLab where the transient voltages are calculated using a rigorous PEEC method. The WT is modeled as a waveguide where distinct propagation modes are considered. In this approach, the aerial parts are not represented by lumped elements of the circuit, and no interface with EMTP-type programs is needed.

II. SOIL MODELING

Soil can be represented by its electrical parameters *i.e.* magnetic permeability (μ_g), resistivity (ρ_g), and relative permittivity (ε_{rg}). The magnetic permeability is equal to the magnetic permeability of free space (μ_0) for most lightning performance studies. However, the resistivity (ρ_g) and relative permittivity (ε_{rg}) are significantly variable with the frequency. This phenomenon is related to the several polarization mechanisms (molecular, ionic, and electronic) in the soil particles as the frequency increases. When the frequency effect is considered, the soil becomes more conductive, and the relative permittivity decreases as the frequency increases. The closed-form expressions for FD soils parameters recommended by CIGRÈ WG are given by [11]

$$\rho_g(f) = \rho_0 \{1 + 4.7 \times 10^{-6} f^{0.54} \rho_0^{0.73}\}^{-1} \quad (1)$$

$$\varepsilon_r(f) = 12 + 9.5 \times 10^4 \rho_0^{-0.27} f^{-0.46} \quad (2)$$

where ρ_0 , in $\Omega\cdot\text{m}$, is the low-frequency resistivity measured at 100 Hz and f , in Hz, is the frequency. The soil resistivity and permittivity are plotted as a surface graph as depicted in Fig.1 in the range of 100 Hz to 5 MHz and low-frequency resistivity ρ_0 of 100 $\Omega\cdot\text{m}$ to 5,000 $\Omega\cdot\text{m}$. The soil resistivity ρ_g is strongly dependent on the frequency, and low-frequency resistivity, where the soil becomes more conductive and the reduction is more noticeable at the high frequencies. The permittivity ε_r decreases for the increasing frequency related to the several polarization mechanisms occurring in the soil particles [11]. These closed-form equations are incorporated at the full-wave electromagnetic software XGSLab [12] used in this work. The voltages are calculated using the Partial

Element Equivalent Circuit (PEEC), based on the thin-wire approximation of the metallic structure (here the WT). This method solves the related Electric Field Integral Equations (EFIE) from the applied Maxwell's equations using the total electric field, currents, and charge densities on a wire surface. Details of PEEC formulation are in Appendix A of [14]. As known in the literature, the interconnected grounding systems provide a lower harmonic impedance, resulting in a lower GPR waveform than those generated for isolated grounding systems [3], [4]. This occurs because the interconnected grids facilitate the dispersion of the lightning currents into the grounding, especially during the transient state [15].

III. NUMERICAL RESULTS

The WF is composed of four WTs whose grounding systems (GS) are interconnected by the bare cables buried in an FD ground as depicted by Fig2-(a). The WT can be divided into four main parts as illustrated in Fig.2-(b). Each part is detailed as follows:

- 1) **Blade:** The blades are represented by three thin down-conductors of 10.6 mm in diameter and length of 80 m, connecting to the nacelle;
- 2) **Nacelle:** The nacelle is made with several steel wires forming a box-like module whose dimensions are depicted in Fig.2-(c);
- 3) **Tower:** The tower is modeled by a fixed tubular cylinder whose dimensions are shown in Fig.2-(d);
- 4) **Grounding system:** The interconnected grounding system (GS) of the wind farm is depicted in Fig.2-(e). The center of each GS is separated by 300 m from each other; the bare connecting cables made of copper have a diameter of 10.6 mm and are buried in a depth of 0.6 m and Each GS of the wind turbine is formed by copper and steel wires with a transversal radius of 5.30 mm, forming concentric rings whose diameters are shown in Fig.2-(f). Moreover, four metallic grounding rods with a length of 3 m are added at the outer ring of the GS. The foundation comprises several reinforced steel bars with 20mm transversal diameter forming the other concentric rings as depicted in Fig.2-(g). The steel bars' relative magnetic permeability (μ_r) equals 300.

A. Transient Ground Potential Rise

To evaluate the impact of the FD soil models on the studied wind farm, the transient ground potential rise (GPR) generated for the two lightning strikes and two values of low-frequency soil resistivity ρ_0 equal to 1,000, and 5,000 $\Omega\cdot\text{m}$. In this context, the lightning strike is modeled as an impulsive current source using the Heidler's function given by [13]

$$I(t) = \frac{I_0}{k} \frac{(t/\tau_1)^n}{1 + (t/\tau_1)^n} e^{-t/\tau_2}, \quad (3)$$

where I_0 , in A, is the current peak, τ_1 , and τ_2 , in s, are the front time and the tail time constants, respectively. The n is the exponent, and k is the correction factor for the peak current. For this study, two types of lightning currents are representative of the first positive impulse (FPI) and subsequent negative impulse (SNI), as detailed in IEC

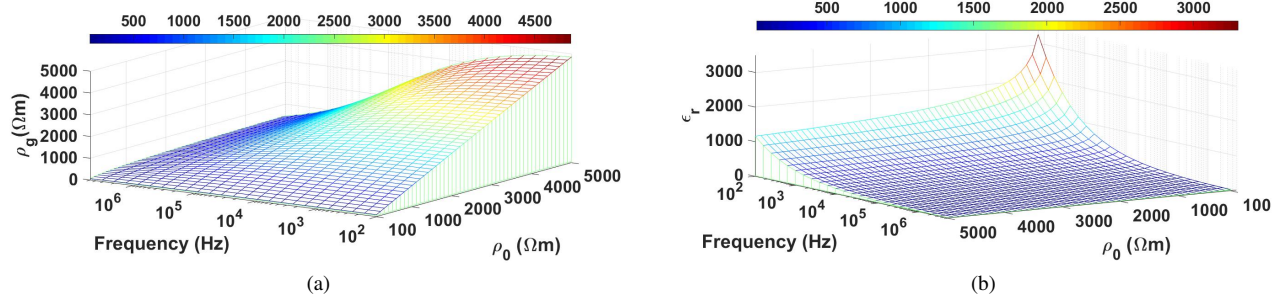


Fig. 1: Soil electrical parameters proposed by CIGRÈ WG [11]: (a) resistivity from (1) and (b) relative permittivity from (2).

62305-1 [13] are used. The lightning parameters of the FPI are: $I_0 = 100$ kA, $\tau_1 = 19$ μs , $\tau_2 = 485$ μs , $n = 10$, $k = 0.93$. For the SNI, the parameters are: $I_0 = 50$ kA, $\tau_1 = 1.82$ μs , $\tau_2 = 285$ μs , $n = 10$, $k = 0.987$ [13]. The employed lightning currents, their derivative waveforms, and their Fourier Transform (magnitude) used in this work are plotted in Fig.3. According to this figure, one notes that the SNI has a shorter front time than the FPI. Furthermore, the subsequent impulse has a higher derivative (around 70 kA/ μs) occurring at 1.8 μs , whereas the maximum for the FPI (around 14 kA/ μs) occurs at 18.6 μs . Additionally, due to the shorter front time of the SNI, a higher frequency content of this current wave is obtained.

The WF comprises four WTs whose GS is interconnected by underground cables buried in FD soils, assuming homogeneous ground of two values of low-frequency ρ_0 resistivity of 1,000 and 5,000 Ωm . The generated GPR at the points **A**, **B**, **C** and **D** (all points located at the tower base) are calculated for the two injected lightning currents at the tip of the blade for the first wind turbine as shown in Fig.2. The GPR waveforms developed for the FPI, and SNI described in (3) are plotted in Fig.4-(a). The GPR waveforms generated at the tower base are calculated for two conditions: First, only the interconnected GS without the WT is assumed, and the obtained results are shown with the label **GS Only**. Second, the WTs are included and connected with each GS, where the lightning strikes at the blade's tip, and the obtained results are shown with the label **GS + Tower**. According to Fig.4, one notes that when only the grounding system is considered-(**GS Only**), the GPR waveforms show noticeably different behavior compared with the condition when the towers are present-(**GS + Tower**). This difference in the GPR waveforms depends on the type of lightning current. Firstly, one observes the propagation effects on the voltage waves along the GS at the points **A**, **B**, **C** and **D**. This phenomenon is evidenced as the GPR presents different peak values associated with distortion of the waveforms and different propagation times along the **A**, **B**, **C** and **D**. The propagation time increases due to the presence of the aerial structures (blade+nacelle+tower), where the voltage waves take an additional time to travel through the structure. The presence of the WT generates GPR waveforms with higher peak values than those assessed with only the interconnected GS. When the WTs are considered, one observes that an oscillatory behavior occurs in the GPR

waveforms generated for the SNI 1/200 μs due to the multiple reflections of propagating waves between the top and base the wind turbine during the transient state [3]. This occurs because the reflection coefficient $k = (Z_g - Z_w)/(Z_g + Z_w)$ at the tower base is negative since grounding impedance of the GS (Z_g) is lower than the surge impedance of the wind turbine (Z_w) [2], [3]. On the other hand, the GPR waveform generated for the FPI has presented smooth behavior due to the lower propagation velocity of this lightning current associated with a larger front-time constant and lower frequency content. After a specific time, these oscillations are mitigated, resulting in smooth behavior for the GPR waveforms, which is ruled by the static resistance GS. To evaluate the impact of the wind turbine on the transient GPR waveforms, the percentage difference is calculated by $\sigma(\%) = (V_A^{GS+T} - V_A^{GS})/V_A^{GS} \times 100\%$, where V_A^{GS+T} and V_A^{GS} is the voltage peak of the GPR waveform with and without the WT at point **A**. The calculated σ is indicated in Fig.4. One notes that the peak values of the GPR waveforms increase with the increase in the soil resistivity since the harmonic impedance of the GS becomes higher, and the presence of long interconnected cables (300 m in this case) increases the inductive effect of the grounding system arrangement of the wind farms[3], [16]. Furthermore, the GPR at points **B**, **C** and **D** also present oscillatory behavior for the SNI 1/200 μs but due to the propagation effect, the amplitude of the oscillations are more reduced than those seen at **A**.

B. Voltage at the tip of the blade

The voltages at the blade tip for both lightning currents FPI and SNI are plotted in Fig.5. According to this figure, the peak values of the voltages at the blade tip have shown no significant difference as the soil resistivity increases during the first instants for the SNI 1/200 μs . However, when the current of FPI is considered, a noticeable difference in the voltage waveforms is seen where the soil of 5,000 Ω presents the highest peak value. At the steady state, one observes a notable difference in the voltage waveforms for both lightning currents, where the highest soil resistivity has shown the most significant variation ruled by the static resistance of the grounding system. The oscillatory voltage behavior at the striking point occurs because of multiple reflections between the tip of the blade from others towers and the grounding system of the WT. Applying the Fourier Transform at the time-domain responses in Fig.5, the transient voltages at the

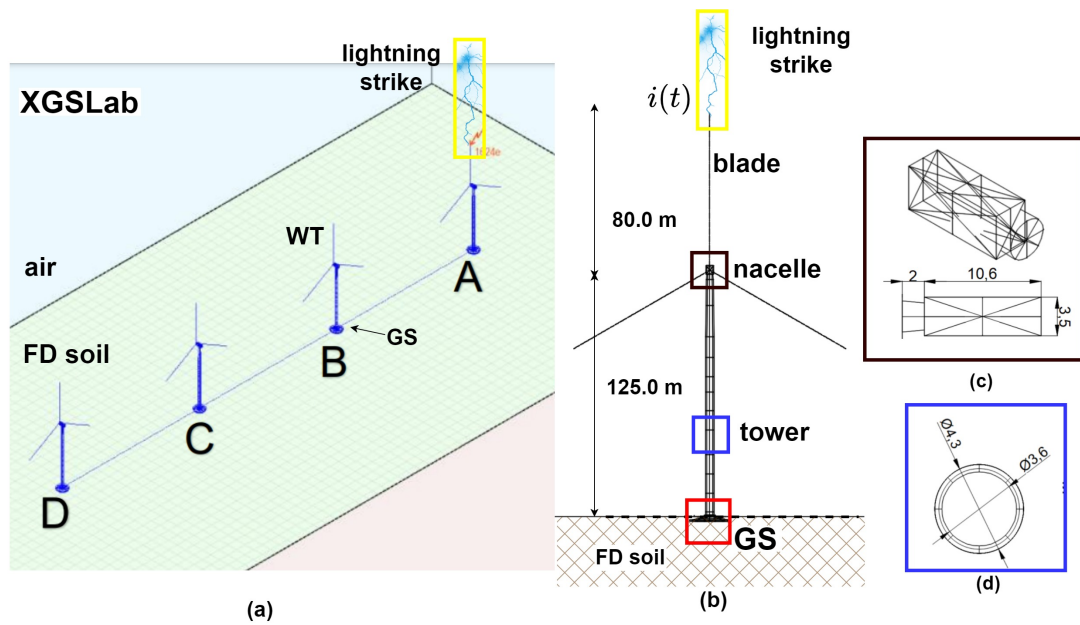


Fig. 2: Wind farm in XGSLab: (a) Configuration of the WT with interconnected GS; (b) Parts of a WT; (c) Nacelle; (d) Tubular tower; (e) Interconnected GS; (f) view of one GS; (g) Foundation. (Not to scale, all dimensions are in meters)

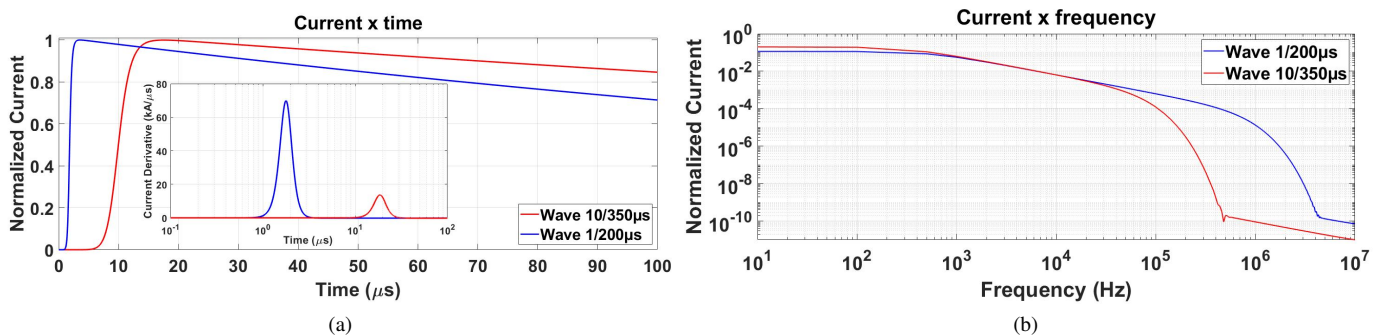


Fig. 3: Injected lightning current waveforms in (a) Time-domain; (b) Frequency domain from its Fourier Transform (Magnitude).

blade's tip in the frequency domain are plotted as shown in Fig.6. Significant differences are seen at the low frequencies, corresponding to pronounced variations at the steady state of the voltage waveforms. At the high frequencies, a resonant peak occurs around 300 kHz related to the height of the wind

turbine (205m from Fig2-(b)).

C. Transient responses at the MVDL

The transient voltages generated at the 34.5-kV medium-voltage distribution line (MVDL) for a lightning

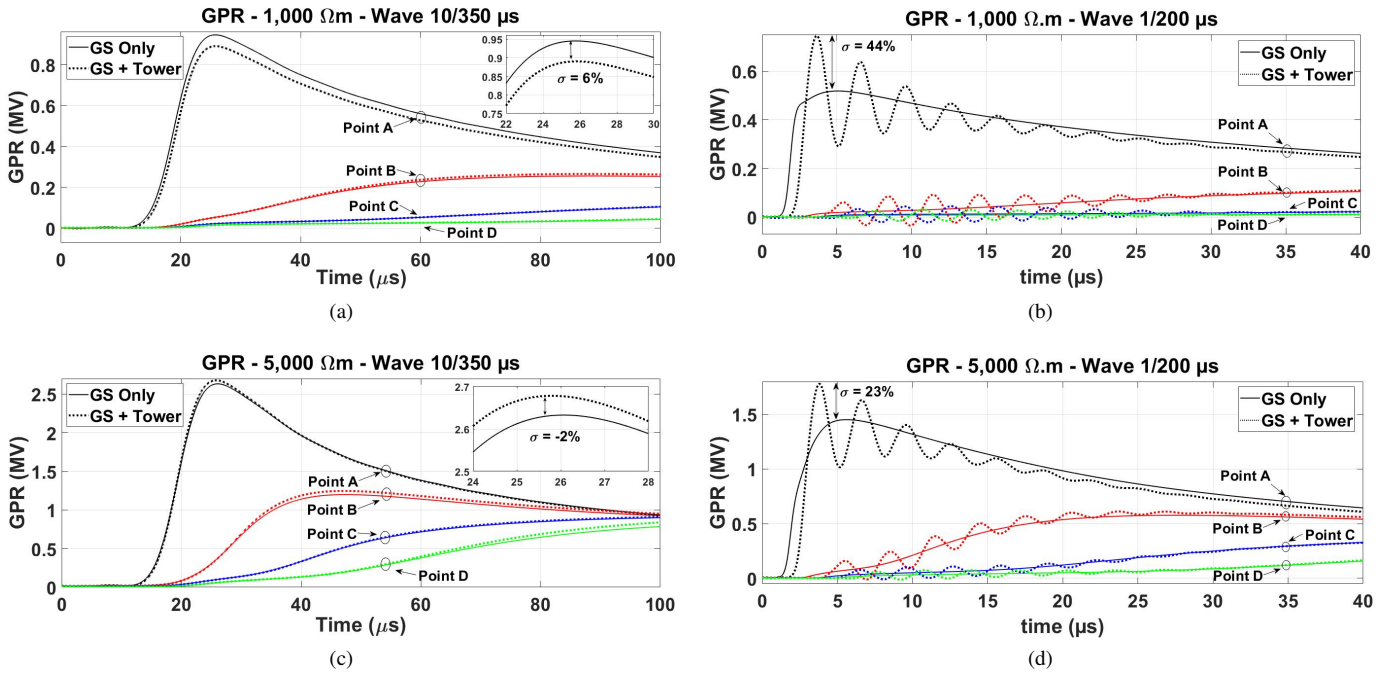


Fig. 4: GPR waveforms generated for the first positive impulse (FPI) 10/350 μ s [left-column side] and for subsequent negative impulse (SNI) 1/200 μ s [right-column side] considering low-frequency resistivity ρ_0 of: (a)-(b) 1,000 and (c)-(d) 5,000 Ω m.

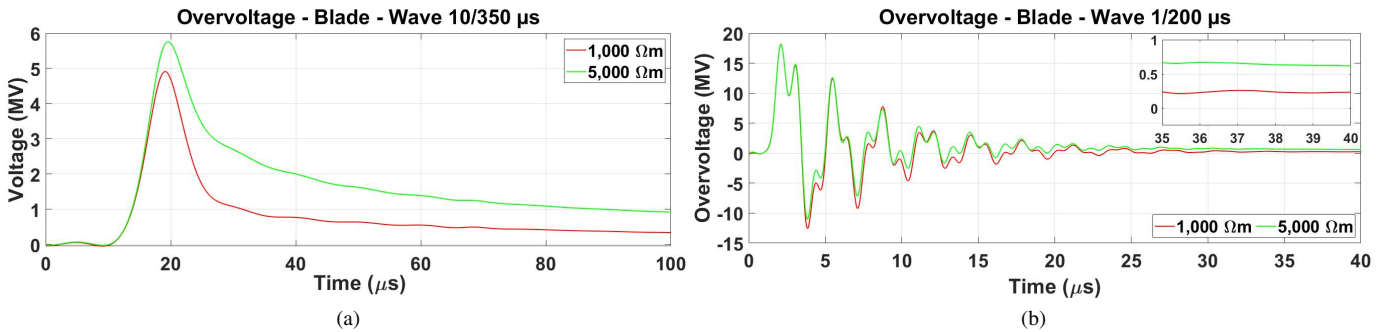


Fig. 5: Voltage waveforms developed at the tip of the blade (striking point) for the: (a) FPI 10/350 μ s (b) SNI 1/200 μ s.

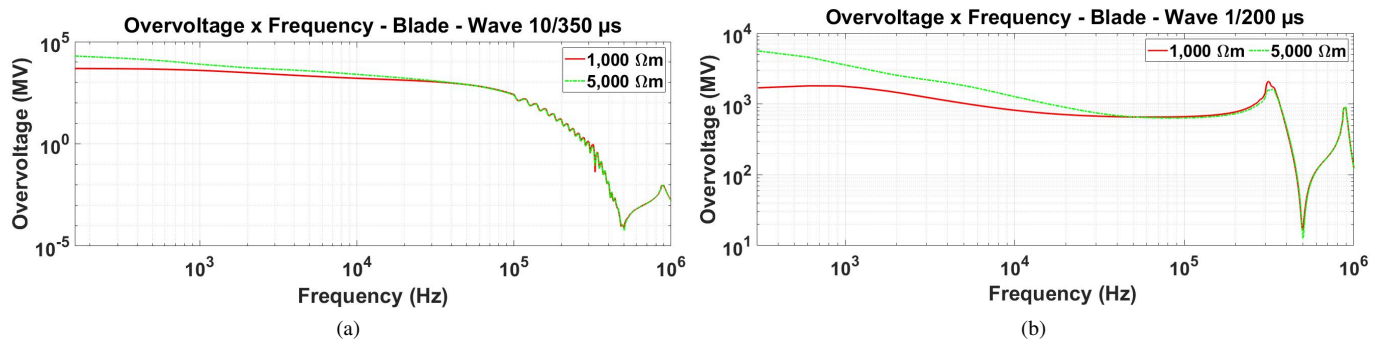


Fig. 6: Fourier transform of the voltage waveforms developed at the striking point for the: (a) FPI 10/350 μ s (b) SNI 1/200 μ s.

strike at the blade's tip are calculated for soils of 1,000 and 5,000 Ω .m. The configuration of the WF with the interconnected grounding system and connected to the medium-voltage distribution line (MVDL) is depicted in

Fig.7. According to this Fig.7-(d), the WF is $\ell = 80$ m from the MVDL, where the pole has a height y of 12m and distance x of 1.05m between the phase conductors (a, b, c), and the total length of the MVDL is 3 km. The phase conductors

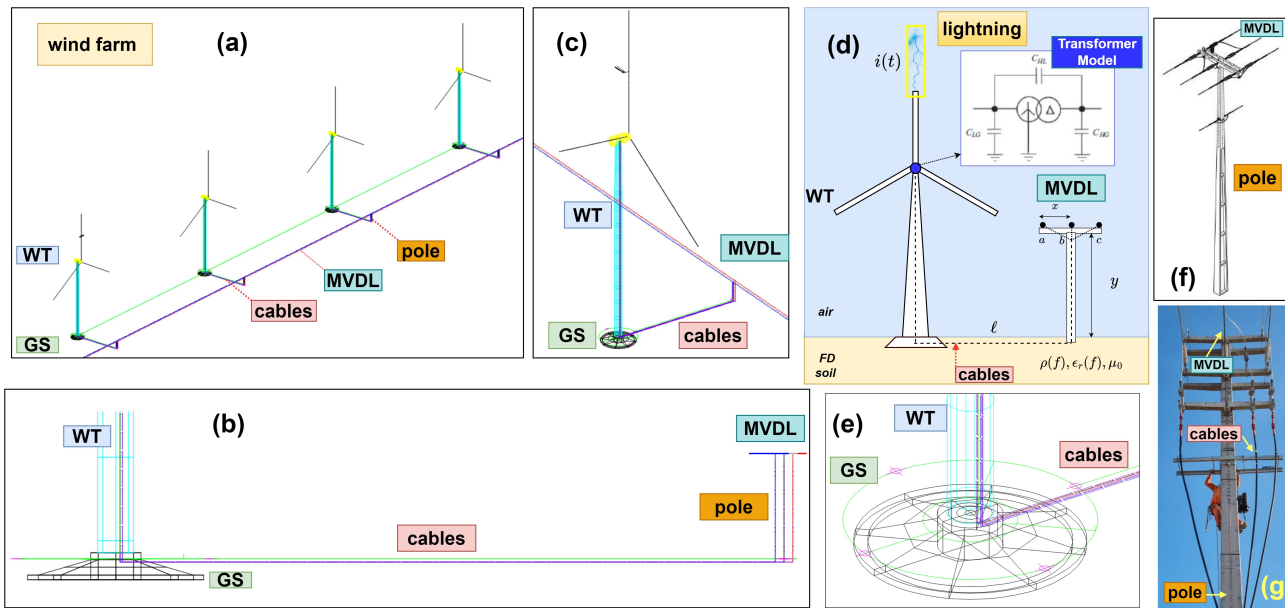


Fig. 7: Medium-voltage distribution Line (MVDL) connected to the wind farm: (a) General view of the wind farm; (b) Details of the wind turbine (WT) foundation and insulated cables to the pole; (c) Details of one WT connected to the MVDL; (d) Illustration of the WT connected to the MVDL and transformer in the nacelle; (e) Grounding system (GS) and insulated cables to the pole; (f) Pole of the MVDL used in this work; (g) Photograph of the MVDL system connected to the insulated cables.

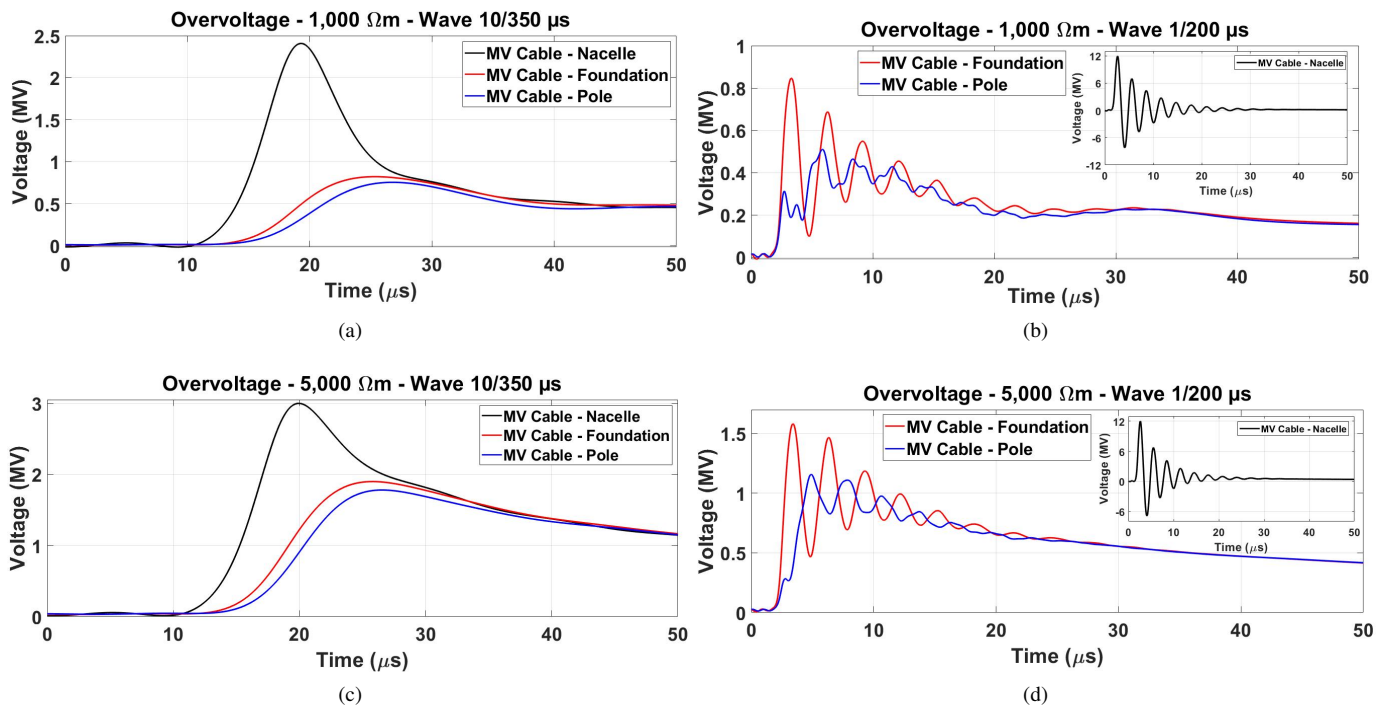


Fig. 8: Overvoltages developed for FPI 10/350μs [left-column side] and SNI 1/200μs [right-column side] for soils with low-frequency resistivity ρ_0 of: (a)-(b) 1,000 and (c)-(d) 5,000 Ωm.

are ACSR Linnet with 336,4 AWG with a cross-section of 198 mm². Additionally, the MVDL is matched at both terminals to avoid reflections from these ends. A dry-type power transformer (0.69/34.5 kV) is installed at the nacelle as depicted in Fig.7-(d) where the C_{LG} and C_{HG} are the capacitances to ground for the low-side voltage (LG) and high-side voltage (HG) whereas C_{HL} is the capacitance

between windings [1]. This study considers the $C_{HG} = 74$ pF. Three insulated cables connect the transformer from the nacelle up to the phase conductors of the MVDL. The cables have a transversal section of 185mm², a screen of 10mm², and insulation formed by EPR. The voltages at the nacelle, foundation (base), and pole for both lightning currents of FPI 10/350μs and SNI 1/200μs are plotted in Fig.8. One

notes that the lightning current waveform and the soil resistivity significantly impact the overvoltage waveforms. Multiple oscillations are observed for SNI 1/200 μ s, where the overvoltage becomes more pronounced as the soil resistivity increases. At the nacelle, the peak values vary from 2.4 MV to 3.0 MV for the FPI for increasing soil resistivity. On the other hand, the peak values of 12 MV are seen at the nacelle for the SNI 1/200 μ s, being practically constant for both soil resistivities. These results are following Nazari[9], where the voltage to the striking point has similar peak values for fast-front disturbances. It is worth mentioning that some protective devices, such as surge arresters, must be installed at the nacelle to avoid these dangerous voltages that may damage the equipment. The overvoltages at the foundation depend strongly on the soil resistivity, affecting the peak values and the propagation time. As observed, the peak value varies from 0.70 MV to around 2.0 MV when the soil resistivity increases from 1,000 and 5,000 Ω m for the FPI 10/350 μ s, besides the distortion of the waveform due to the propagation effect along the cable. The voltages at the pole (at the receiving end of the cable-see Fig.7-(f)) have similar behavior when the FPI 10/350 μ s is considered, only differing for more pronounced distortion in the waveforms. The voltages in the foundation and pole for the SNI 1/200 μ s present multiple oscillations due to induced effects of the lightning currents flowing from the striking point to the grounding system; These flowing currents into the grounding system generate magnetic fields that induce electromagnetic forces to cables in the nacelle. Besides that, these magnetic fields can cause interference with the communication or control systems which may lead to malfunctions of equipment [1].

IV. CONCLUSIONS

This paper investigated the transient voltages generated on a WT and a medium-voltage distribution line connected to a WF with interconnected grounding systems. The voltages are calculated assuming that one wind turbine is struck by lightning. The full system (WF and medium-voltage distribution line) was modeled using the full-wave electromagnetic software XGSLab[®], and the voltages on these components were computed employing the numerical method PEEC, assuming FD soils of 1k and 5k Ω .m. The responses were assessed for lightning currents of FPI (100-kA 10/350 μ s) and SNI (50-kA, 1/200 μ s). Results indicated that when the aerial elements are considered, the GPR developed for the SNI contains an oscillatory behavior due to the multiple reflections between the blade tip and the wind turbines' base. These oscillations are not seen for the FPI due to the lower propagation velocity for this lightning current. These peak values of GPR increase notably as the soil resistivity increases. Concerning the voltages at the blade, the first microseconds have shown no significant variation for the subsequent impulse. However, notable differences are seen in the steady state ruled by the static resistance of the grounding system for both lightning currents. Finally, the overvoltages developed at the MVDL significantly depend on the soil resistivity and lightning current waveform. The

induced magnetic field can cause malfunctions and damage the equipment at the nacelle. As a contribution, the XGSLab modeled a real WF with an MVDL system by the thin-wire approach and considered the WTs as waveguides with distinct propagation modes for a wide frequency spectrum associated with the largely used PEEC. This approach does not use any lumped-circuit approach for the aerial elements of the wind turbines incorporated in EMTP-type programs.

REFERENCES

- [1] A. Piantini, *Lightning Interaction with Power Systems: Applications, Volume 2*, ser. Energy Engineering. Institution of Engineering and Technology, 2020. [Online]. Available: <https://books.google.com.br/books?id=pFvUDwAAQBAJ>
- [2] K. Yamamoto, T. Noda, S. Yokoyama, and A. Ametani, "Experimental and analytical studies of lightning overvoltages in wind turbine generator systems," *Electric Power Systems Research*, vol. 79, no. 3, pp. 436–442, 2009.
- [3] R. Alipio, M. Guimarães, L. Passos, D. Conceição, and M. T. C. de Barros, "Ground potential rise in wind farms due to direct lightning," *Electric Power Systems Research*, vol. 194, p. 107110, 2021.
- [4] A. Sunjerga, Q. Li, D. Poljak, M. Rubinstein, and F. Rachidi, "Isolated vs. interconnected wind turbine grounding systems: Effect on the harmonic grounding impedance, ground potential rise and step voltage," *Electric Power Systems Research*, vol. 173, pp. 230–239, 2019.
- [5] X. Zhang, Y. Zhang, and X. Xiao, "An improved approach for modeling lightning transients of wind turbines," *International Journal of Electrical Power & Energy Systems*, vol. 101, pp. 429–438, 2018.
- [6] R. Araneo and S. Celozzi, "Transient behavior of wind towers grounding systems under lightning strikes," *International Journal of Energy and Environmental Engineering*, vol. 7, no. 2, pp. 235–247, 2016.
- [7] D. S. Gazzana, A. Smorgonskiy, N. Mora, A. Šunjerga, M. Rubinstein, and F. Rachidi, "An experimental field study of the grounding system response of tall wind turbines to impulse surges," *Electric Power Systems Research*, vol. 160, pp. 219–225, 2018.
- [8] Z. Chen, "Issues of connecting wind farms into power systems," in *2005 IEEE/PES Transmission & Distribution Conference & Exposition: Asia and Pacific*. IEEE, 2005, pp. 1–6.
- [9] M. Nazari, R. Moini, S. Fortin, F. P. Dawalibi, and F. Rachidi, "Impact of frequency-dependent soil models on grounding system performance for direct and indirect lightning strikes," *IEEE Transactions on Electromagnetic Compatibility*, vol. 63, no. 1, pp. 134–144, 2021.
- [10] W. C. Da Silva, W. L. M. De Azevedo, J. L. A. D'Annibale, A. R. J. De Araújo, and J. P. Filho, "Analysis on induced voltages in wind farms close to distribution lines on frequency-dependent soil," in *2022 IEEE Power Energy Society General Meeting (PESGM)*, 2022, pp. 1–5.
- [11] CIGRE-WG4.33, "Impact of soil-parameter frequency dependence on the response of grounding electrodes and on the lightning performance of electrical systems," *Technical Brochure 781*, 2019.
- [12] XGSLab, "Electromagnetic simulation for power, grounding and lightning protection systems." [Online]. Available: <https://www.xgslab.com/xgslab-new/general>
- [13] IEC Webstore International Electrotechnical Commission, "Iec61400-24:2019 wind energy generation systems part 24: Lightning protection," 2019.
- [14] P. Yutthagowith, A. Ametani, N. Nagaoka, and Y. Baba, "Application of the partial element equivalent circuit method to analysis of transient potential rises in grounding systems," *IEEE Transactions on Electromagnetic Compatibility*, vol. 53, no. 3, pp. 726–736, 2011.
- [15] O. Kherif, S. Chiheb, M. Teguvar, and A. Mekhaldi, "Impulse analysis of isolated and interconnected wtgss under lightning discharges," *IJEEES Trans. High Volt.*, vol. 0, pp. 21–27, 2018.
- [16] W. L. M. de Azevedo, A. R. J. de Araújo, J. S. L. Colqui, J. L. A. D'Annibale, and J. P. Filho, "Alternative study to reduce backflashovers using tower-footing grounding systems with multiple inclined rods," *Electric Power Systems Research*, vol. 214, p. 108893, 2023.